Structural Engineering and Mechanics, *Vol. 46, No. 5 (2013) 673-693*
DOI: http://dx.doi.org/10.12989/sem.2013.46.5.673

Experimental calibration of forward and inverse neural networks for rotary type magnetorheological damper

Subrata Bhowmik[1a], Felix Weber[*2] and Jan Høgsberg[1b]

[1]*Department of Mechanical Engineering, Technical University of Denmark, Lyngby 2800, Denmark*
[2]*Empa, Swiss Federal Laboratories for Materials Science and Technology, Structural Engineering Research Laboratory, 8600 Dübendorf, Switzerland*

(Received September 1, 2011, Revised April 30, 2013, Accepted May 2, 2013)

Abstract. This paper presents a systematic design and training procedure for the feed-forward back-propagation neural network (NN) modeling of both forward and inverse behavior of a rotary magnetorheological (MR) damper based on experimental data. For the forward damper model, with damper force as output, an optimization procedure demonstrates accurate training of the NN architecture with only current and velocity as input states. For the inverse damper model, with current as output, the absolute value of velocity and force are used as input states to avoid negative current spikes when tracking a desired damper force. The forward and inverse damper models are trained and validated experimentally, combining a limited number of harmonic displacement records, and constant and half-sinusoidal current records. In general the validation shows accurate results for both forward and inverse damper models, where the observed modeling errors for the inverse model can be related to knocking effects in the measured force due to the bearing plays between hydraulic piston and MR damper rod. Finally, the validated models are used to emulate pure viscous damping. Comparison of numerical and experimental results demonstrates good agreement in the post-yield region of the MR damper, while the main error of the inverse NN occurs in the pre-yield region where the inverse NN overestimates the current to track the desired viscous force.

Keywords: experimental validation; inverse MR damper model; rotary MR damper; neural network

1. Introduction

Magnetorheological (MR) dampers used for controlled damping of structural vibrations have received considerable attention during the last decades because they offer the possibility to adapt their semi-active force in real-time to the structural vibrations (Christenson *et al.* 2006, Li *et al.* 2007, Neelakantan and Washington 2008, Wu and Cai 2010). MR dampers are suitable for mitigation of vibrations in large civil engineering structures because they combine large control force ranges, low power requirements, fast response time and fail safe performance (Spencer and Nagarajaiah 2003).

Basically, rotary type magnetorheological (MR) dampers consist of a housing that includes the

∗Corresponding author, Ph.D., E-mail: felix.weber@empa.ch
[a]Ph.D., E-mail: subho@mek.dtu.dk
[b]Professor, E-mail: jhg@mek.dtu.dk

http://www.techno-press.org/?journal=sem&subpage=8 ISSN: 1225-4568 (Print), 1598-6217 (Online)

MR fluid and the rotating part of the disc. The MR fluid is a suspension of oil with magnetizable particles with average diameter of 5 μm and some additives. The particles and the ferromagnetic parts of the housing and disc are magnetized by the magnetic field that is produced by two coils which are installed within the housing on both sides of the disc. The magnetized particles build chains and thereby stick to the disc and housing (Weber and Boston 2011a). When the disc starts to rotate the particle chains are initially stretched before they start to slide relative to the surfaces of the disc and/or the housing. The particle chains may also break, whereby rupture between particles occurs. The phase where particle chains are elastically stretched is commonly denoted as the pre-yield region of the MR fluid, while the sliding phase is called the post-yield region. The particle chains start to slide when the dry friction force between particles or between particle chains and disc or between particle chains and housing is balanced by the elastic force due to elongation of the particle chains (Weber and Boston 2011a). Since this sticking depends strongly on the magnetization of the MR fluid, and thereby on the MR damper current, the post-yield force of the MR damper typically exhibits a strong current dependency. Because the superposed viscous force is usually rather small and the MR fluid viscosity depends only slightly on the coil current, the applied current primarily controls the friction force of the MR damper, while the viscous force component is mainly governed by the rotating speed of the disc and the inherent viscosity of the MR fluid (Weber *et al.* 2008, Weber and Boston 2011a). In order to be able to control the total MR damper force relative to a desired control force, the coil current must be modulated so that the control force tracking error is acceptable. Due to the non-linear behavior of the MR damper force, i.e. the non-linear relation between current and sticking force and the non-linear dependency of the MR fluid viscosity on current, force tracking with force feedback only may fail to track the desired force accurately. Therefore, model-based feed forward control schemes are needed to solve the force tracking task with sufficient accuracy (Weber and Boston 2011b, Weber *et al.* 2011c). Such approaches can then later be extended by a force feedback in order to further decrease the remaining force tracking error (Weber and Maslanka 2012).

MR dampers are either operated at zero or constant current, which are called passive-off or passive-on strategies (Weber *et al.* 2005), or they are controlled in real-time within a particular feedback loop (Maslanka *et al.* 2007, Weber *et al.* 2009). In the latter case the structural response is typically measured at damper position and the MR damper current is controlled in real-time to obtain minimum tracking error with respect to a desired control force. The force tracking task is usually solved by a model-based feed forward control scheme, simply to avoid costly force sensors (Maslanka *et al.* 2007, Weber *et al.* 2009). The input states of the feed forward controller may be the damper displacement, velocity, acceleration, or any combination of these states, and the desired control force, while the output state is the desired MR damper current. In practice the desired current is realized by a current driver, which compensates for the coil impedance dynamics of the MR damper. Therefore, an inverse MR damper model is required that estimates the desired damper current based on a limited number of the above mentioned input states. This model is usually referred to as an inverse MR damper model (Tse and Chang 2004, Yang *et al.* 2004, Dominguez *et al.* 2006, Weber and Boston 2011b, Weber *et al.* 2011c, Weber and Maslanka 2012) because it predicts the controllable damper current, while the classic forward models predict the damper force.

Many parametric and non-parametric forward models for classic cylindrical type MR dampers have been presented in the literature. Some of the prominent parametric approaches are the Bouc-Wen model, which captures both the pre- and post-yield regions (Yang *et al.* 2004, Dominguez *et al.* 2006), the Bingham model which basically represents current dependent friction (Ikhouane and

Dyke 2007), the Dahl model which describes an elasto-plastic material behavior with supplemental viscous effects (Shulman *et al.* 2006) and the LuGre approach that models the MR fluid particle chains as brushes with sticking and sliding against the damper housing (Jiménez and Alvarez-Icaza 2005, Yang *et al.* 2009, Boston *et al.* 2010). These models have also been extended by additional stiffness, viscous and mass elements to account for the accumulator behavior, the current dependent viscous force and the inertia of the damper piston and other accelerated parts (Sahin *et al.* 2010). The parameters for minimum model error are typically obtained from the test data directly (Sims *et al.* 2004, Weber *et al.* 2008) or by a numerical optimization tool (Ye and Wang 2007). Once calibrated, these parametric approaches can be used as observers to solve the force tracking problem without feedback from a force sensor (Maslanka *et al.* 2007, Weber and Boston 2011b, Weber 2013a).

Non-parametric models are mainly based on fitted polynomials (Weber *et al.* 2009), genetic algorithms (Xiaomin *et al.* 2009), fuzzy logic (Tsoukalas and Uhrig 1997, Won and Sunwoo 2009), neural networks (NN) (Chang and Roschke 1998, Xia 2003, Chang and Zhou 2002, Wang and Liao 2005, Lee *et al.* 2008, Metered *et al.* 2009, Weber *et al.* 2013b) or hybrid approaches (Soeiro *et al.* 2008). As demonstrated in Chang and Roschke (1998) the NN approach is able to model the forward MR damper behavior fairly accurate. Most of the NNs are trained with simulated input-output data, usually generated by the Bouc-Wen model, as e.g., in Wang and Liao (2005). Only few NN have been trained with experimental data (Metered *et al.* 2009), containing system noise and knocking effects due to bearing tolerances. This makes the training of the network much more difficult, and appropriate filtering of the training data during post processing can be very crucial for the NN performance. The NN architecture is usually found by a trial and error method, and the resulting NN architecture is therefore not necessarily optimal with respect to the minimization of the modeling error.

The present investigation provides a systematic approach to the design and calibration of NNs for both the forward and inverse behavior of a rotary type MR damper based on experimentally measured training data. It is shown that only force, velocity and current, with necessary previous states, are sufficient for the construction of effective NN architectures. For the NN based inverse modeling of the MR damper the absolute value of velocity and damper force are used as input training data. This modification of taking the absolute value in the training data input has a major influence on the proper estimation of the current because the current is always positive, irrespective of the sign of the training inputs. Moreover, the MR damper behavior is measured at constant and half-sinusoidal current, where the half-sinusoidal current tests are performed because they generate training data very similar to the current records associated with damping of structures excited at resonance. The experimental data is filtered so that potential noise is minimized and any offset values are removed. In this paper a semi-systematic approach for the calibration of the NN architecture based on the minimization of the associated modeling error is described. The architecture of the NNs for both the forward and the inverse MR damper models are presented and validated with measurement data independent of the training data. Good accuracy is generally reported, and the validated inverse and forward models are subsequently used in numerical simulations, where pure viscous damping is reproduced in real-time.

The paper is structured as follows: Section 2 describes the collection of the training data including the filtering and post-processing of the training data, section 3 explains the design and training of the NN architectures, section 4 shows the model validation and discusses the obtained results and section 5 tests the forward and inverse MR damper models by real-time tracking of viscous damping.

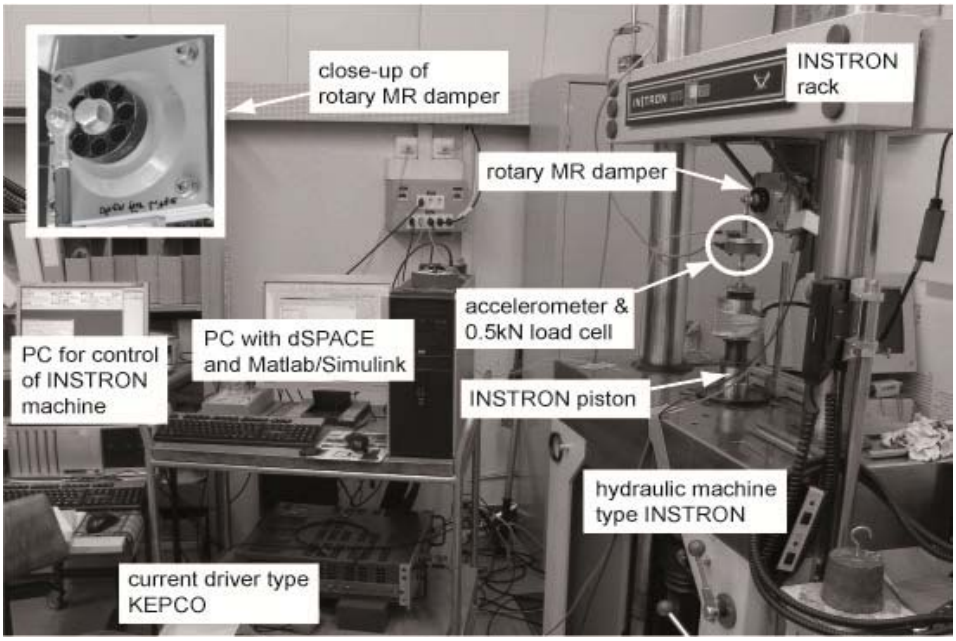

Fig. 1 Experimental set-up with rotary MR damper in hydraulic test machine

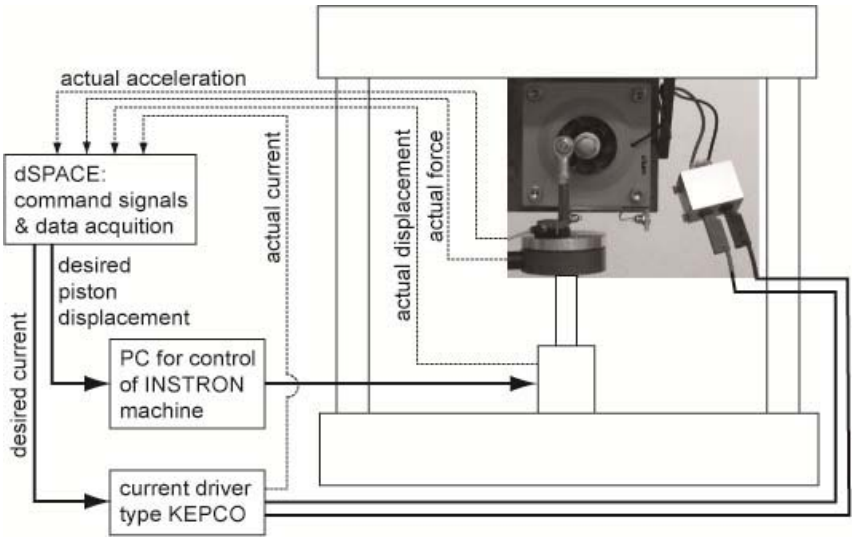

Fig. 2 Schematic of test set-up

2. Experimental data

Section 2.1 introduces the experimental test set-up used to obtain the MR damper response data used for training of the NN, while the necessary post-processing of the measured time histories is described in section 2.2.

Table 1 Measurement data for training of NN and model validation

set for training	set for validation	desired displacement	desired current
1a	1b	sin, 5 mm, [0.5, 1.0, 1.27, 1.8, 2.2] Hz	0 A
2a	2b	sin, 5 mm, [0.5, 1.0, 1.27, 1.8, 2.2] Hz	1 A
3a	3b	sin, 5 mm, [0.5, 1.0, 1.27, 1.8, 2.2] Hz	2 A
4a	4b	sin, 5 mm, [0.5, 1.0, 1.27, 1.8, 2.2] Hz	3 A
5a	5b	sin, 5 mm, [0.5, 1.0, 1.27, 1.8, 2.2] Hz	4 A
6a	6b	sin, 10 mm, [0.5, 1.0, 1.27, 1.8, 2.2] Hz	0 A
7a	7b	sin, 10 mm, [0.5, 1.0, 1.27, 1.8, 2.2] Hz	1 A
8a	8b	sin, 10 mm, [0.5, 1.0, 1.27, 1.8, 2.2] Hz	2 A
9a	9b	sin, 10 mm, [0.5, 1.0, 1.27, 1.8, 2.2] Hz	3 A
10ae	10b	sin, 10 mm, [0.5, 1.0, 1.27, 1.8, 2.2] Hz	4 A
11a	11b	sin, 5 mm, [0.5, 1.0, 1.27, 1.8, 2.2] Hz	half-sin, 0 A, [0.5, 1.0, 1.27, 1.8, 2.2] Hz
12a	12b	sin, 5 mm, [0.5, 1.0, 1.27, 1.8, 2.2] Hz	half-sin, 1 A, [0.5, 1.0, 1.27, 1.8, 2.2] Hz
13a	13b	sin, 5 mm, [0.5, 1.0, 1.27, 1.8, 2.2] Hz	half-sin, 2 A, [0.5, 1.0, 1.27, 1.8, 2.2] Hz
14a	14b	sin, 5 mm, [0.5, 1.0, 1.27, 1.8, 2.2] Hz	half-sin, 3 A, [0.5, 1.0, 1.27, 1.8, 2.2] Hz
15a	15b	sin, 5 mm, [0.5, 1.0, 1.27, 1.8, 2.2] Hz	half-sin, 4 A, [0.5, 1.0, 1.27, 1.8, 2.2] Hz
16a	16b	sin, 10 mm, [0.5, 1.0, 1.27, 1.8, 2.2] Hz	half-sin, 1 A, [0.5, 1.0, 1.27, 1.8, 2.2] Hz
17a	17b	sin, 10 mm, [0.5, 1.0, 1.27, 1.8, 2.2] Hz	half-sin, 2 A, [0.5, 1.0, 1.27, 1.8, 2.2] Hz
18a	18b	sin, 10 mm, [0.5, 1.0, 1.27, 1.8, 2.2] Hz	half-sin, 3 A, [0.5, 1.0, 1.27, 1.8, 2.2] Hz
19a	19b	sin, 10 mm, [0.5, 1.0, 1.27, 1.8, 2.2] Hz	half-sin, 4 A, [0.5, 1.0, 1.27, 1.8, 2.2] Hz

2.1 Experimental set-up

The MR damper under consideration is a rotary type MR damper with a maximum current of 4 A. The damper is shown in Fig. 1 and further details on the damper characteristics can be found in Weber *et al.* (2008) and Boston *et al.* (2010). At constant current the damper behaves almost as a friction damper, with only a small velocity dependency. The apparent friction force level is approximately 30 N at 0 A and 300 N at 4 A. Details concerning the behaviour of the rotary type MR damper have been explained in the previous section. The training and the validation data are obtained from forced displacement tests using a hydraulic testing machine of type INSTRON, see Fig. 1. The desired piston displacement is defined in Matlab®, processed real time by a dSPACE® DS1104 R&D controller board and finally send as a command signal directly to the INSTRON PC unit. A flow diagram of the experimental setup is shown in Fig. 2. The actual displacement is captured directly as output from the INSTRON machine and acquired by the dSPACE® system at 1000 Hz sampling frequency. The desired MR damper current is also defined in Matlab/dSPACE®, and tracked real time by a KEPCO current driver. The actual damper current is measured by the KEPCO amplifier and acquired by the dSPACE® system. The MR damper force is measured by a 500 N load cell, and the acceleration of the piston is also measured for verification and potential later use in connection with training or validation. Furthermore, acceleration is suitable for detection of the knocking effects due to the finite bearing tolerances of 0.01-0.02 mm of the joints of the damper rod. A summary of the tests conducted is provided in Table 1. Each test is performed twice: The first set is used as training data, while the second completely independent set is used to validate the NN models. Tests 1-10 are performed at

constant current, while tests 11-19 are conducted with half-sinusoidal current. As seen in Table 1 the desired displacement is pure sinusoidal, combining amplitudes of 5 mm and 10 mm, and frequencies from 0.5 Hz to 2.2 Hz.

2.2 Post processing of experimental data

Initially, the measurement data is post-processed by a low pass filter in order to avoid that the NN is trained by high frequency signal components, e.g. noise and knocking effects, which are typically of no interest. The applied low pass filter has the following properties:

· Digital Butterworth low pass filter.
· Filter order 2.
· Cut-off frequency 100 Hz.

Any offset in the displacement, acceleration and force signals are removed by simply balancing positive and negative maxima during steady state conditions. The effect of the filtering of displacement, acceleration, damper current and damper force is shown in Fig. 3. As seen in Figs. 3(a) and (c) the high-frequency signal parts in the displacement and damper current are effectively removed by the filter, and the main task is basically to avoid a too significant change in the phase and reduction in the peak values. The acceleration is very sensitive to the various sources of noise, and the influence of the filter therefore becomes very evident in Fig. 3(b). The damper force is shown in Fig. 3(d) where the main modification is the removal of the offset level. Note that the constant force level at zero crossing is due to the previously mentioned bearing tolerance. The effect is mainly visible in the acceleration signal, which is also shown in Fig. 3(d).

The training of the NN also requires the damper velocity $\dot{x}$, which is not directly measured. It is instead estimated at each time instant k by numerical differentiation of the displacement x as

$$\dot{x}(k) = \left(\frac{x(k) - x(k-1)}{t(k) - t(k-1)} \right) \quad \text{with initial condition} \quad \dot{x}(1) = 0 \tag{1}$$

The inherent noise resulting from the numerical differentiation is subsequently removed by the following low pass filter:

· Digital Butterworth low pass filter.
· Filter order 2.
· Cut-off frequency 20 Hz.

Fig. 4(a) shows the velocity record obtained by differentiation of the sinusoidal displacement with amplitude 5 mm and frequency 1 Hz. The amplitude of the velocity is 31 mm/s, which agrees well with the analytical value of 2π (1Hz) (5 mm) = 31.4 mm/s. The figure also shows the corresponding displacement, and it is observed that the phase shift between displacement and velocity is the expected one quarter of a period. Fig. 4(a) therefore indicates that the method in Eq. (1) leads to a velocity signal with correct amplitude and phase compared to the associated displacement. After the signal post processing, 10 steady state cycles of the data sets 1-19 in Table 1 are isolated and then connected after each other to get individual continuous time histories for displacement, velocity, acceleration, current and force, respectively. Fig. 4(b) shows the combination system for the generation of the resulting time histories used for training of the NN. It should be noted that the sets are always connected at zero crossings of the displacement. To have a reasonably limited amount of data for the training of the NN the time histories are finally down sampled from 1000 Hz to 200 Hz.

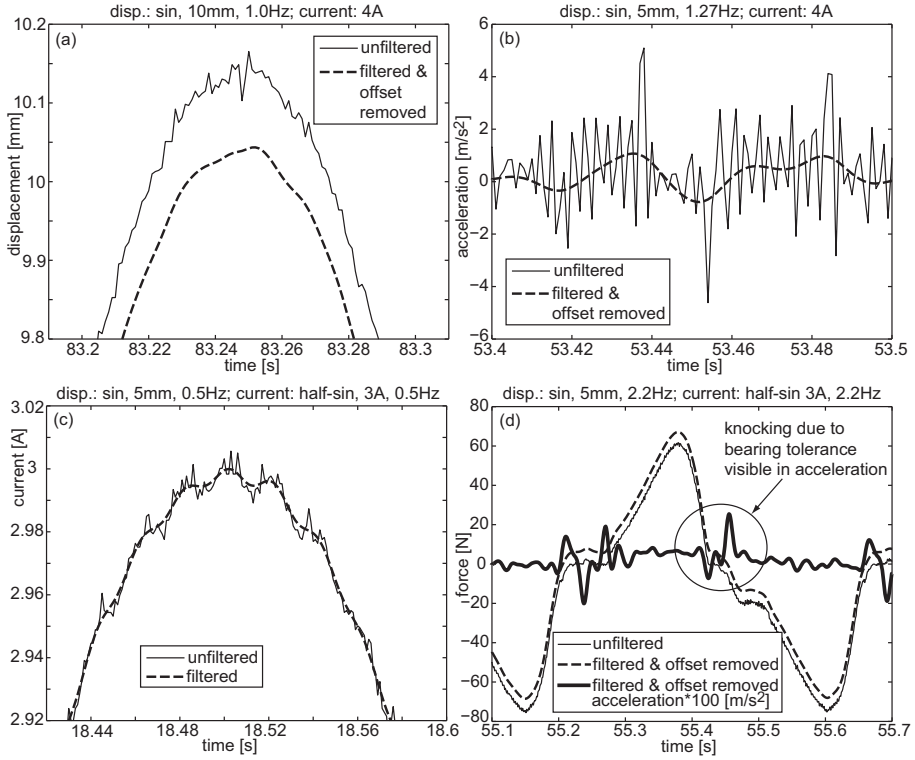

Fig. 3 Filtering of measurement data

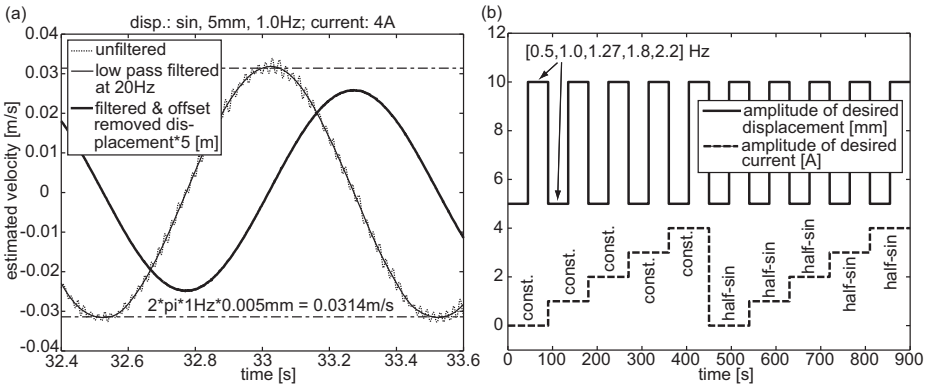

Fig. 4 Estimated velocity (a) and training data time history (b)

3. Modeling

The modeling of a system using the NN tool requires the following basic three steps: (a) measurement of the input and output states of the system under consideration (see previous section), (b) choosing the architecture of the particular NN, which is described in section 3.1, and (c) training the chosen architecture with the measurement data that is described in section 3.2 for the forward MR damper model and in section 3.3 for the inverse MR damper model.

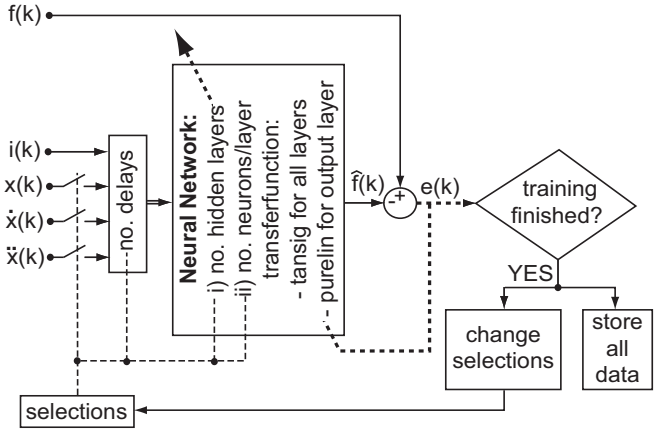

Fig. 5 Procedure to find suboptimal NN architecture

3.1 NN architecture

The NN architecture is characterized by:

· What states are used as input.
· How many previous values of the input states are used.
· The number of hidden layers and neurons per layer.
· The transfer functions of each layer.

Because of the large variety of modeling parameters, the trial and error method is often applied to find an NN architecture with acceptable modeling errors. Using the trial and error approach the training yields the best parameters for the chosen NN architecture, but not necessarily the best NN architecture with the best parameters. In the present work, a semi-systematic approach is used to obtain a near optimal NN architecture. The procedure is illustrated schematically in Fig. 5. A number of NN are trained to model the forward MR damper behavior with the current records and one, or several, of the time histories for displacement, velocity and acceleration as input states. The number of previous states, the number of hidden layers and neurons are also varied. The literature shows that the log-sigmoidal transfer function is commonly used for the hidden layers in multilayer networks that are trained using the back propagation method because this transfer function is differentiable and gives the best result for the minimum value and the linear function is used for the output layer because it gives the best maximum value of all the minimum values from the hidden layers. However, since the transfer function of the MR damper behavior, i.e. the force velocity trajectory, is symmetrical about the origin, the log-sigmoidal transfer function might not be one of the best choices. Therefore, the tangent sigmoid transfer function is chosen here for the hidden layers. All trained NN candidates are determined by the Levenberg-Marquardt optimization method, using the *error*(k) between the target force $f(k)$ and the estimated force $\hat{f}(k)$ by back propagation. When the training is finished, the individual NN architecture is stored and a new NN architecture is trained for different input properties. After all possible combinations of input data have been used for training of the NN architecture, the particular NN architecture with the smallest modeling error is identified as the best NN architecture, and stored for subsequent analyses. This systematic optimization strategy shows the following trends:

1. Velocity and damper current are mandatory input states. This is also confirmed by the large

number of parametric MR damper models that are based on velocity and current as input states (Dominguez *et al.* 2004, Maslanka *et al.* 2007, Aguirre *et al.* 2010, Weber and Boston 2011b).
2. Using acceleration as additional input seems to increase the noise in the estimated force without improving the model accuracy.
3. Using displacement as additional input does not decrease the modeling error. This can be explained by the fact that the velocity is determined from displacement by Eq. (1) and because the rotary MR damper has no accumulator and therefore no significant stiffness component.
4. Using both displacement and acceleration as additional input has no influence on the modeling error.
5. It seems that including three previous values, two hidden layers and six neurons per hidden layer provides a suitable compromise between modeling error and computational effort.

3.2 Forward damper model

The NN architecture that is found to minimize the error of the forward MR damper model is based on velocity and damper current as input states, three previous values and two hidden layers of six neurons each. The architecture of the forward NN is shown in Fig. 6. The transfer function $g^{(j)}$ of the neurons of the two hidden layers are selected as a tangent sigmoid function, while the transfer function of the single output layer, i.e., layer 3, is selected as a linear function. If $N^{(j)}$ is the number of neurons in the j^{th} layer then $N^{(3)} = 1$, since the output layer has only a single signal output. Let $O_l^{(0)}$ be the $R\times1$ column vector comprising the signal inputs to the first hidden layer. In the present case $R = 8$ because of the two input variables: velocity and current, both with a current state value and three previous values. The subscript l denotes the individual neurons of the particular layer. Let $O_l^{(j)}$ be the $N^{(j)} \times 1$ vector comprising the signal outputs of the j^{th} layer, which means that the output layer is represented by $O_l^{(3)}$. For the two hidden layers and the single output layer the output is computed as

$$O_l^{(j)} = g^{(j)}(w_l^{(j)} O_l^{(j-1)} + b_l^{(j)}), \quad j = 1, 2, 3 \tag{2}$$

where $g^{(j)}$ is the tangent sigmoid function for the hidden connections with $j = 1, 2$, while it is the linear function for the output connection with $j = 3$. The vector $w_l^{(j)}$ contains the weights of the neural connections, while $b_l^{(j)}$ is the bias vector of the j^{th} layer, which is zero in the present application. Each of the transfer functions operates on the respective element of the vector argument. Thus, the estimation of the damper force by the NN can be expressed as

$$\hat{f}(k) = NN\begin{bmatrix} \dot{x}(k) & \dot{x}(k-1) & \dot{x}(k-2) & \dot{x}(k-3) \\ i(k) & i(k-1) & i(k-2) & i(k-3) \end{bmatrix} \tag{3}$$

where $NN[\ldots]$ represents the computation by the neural network and $i(k)$ denotes the current at time k. For feed forward neural network based forward dynamics modeling, the network output is $\hat{f}(k) = O_l^{(3)}$ whereby $\hat{f}(k)$ is the predicted force from the forward MR model at current time state k. The target of the forward neural network model is

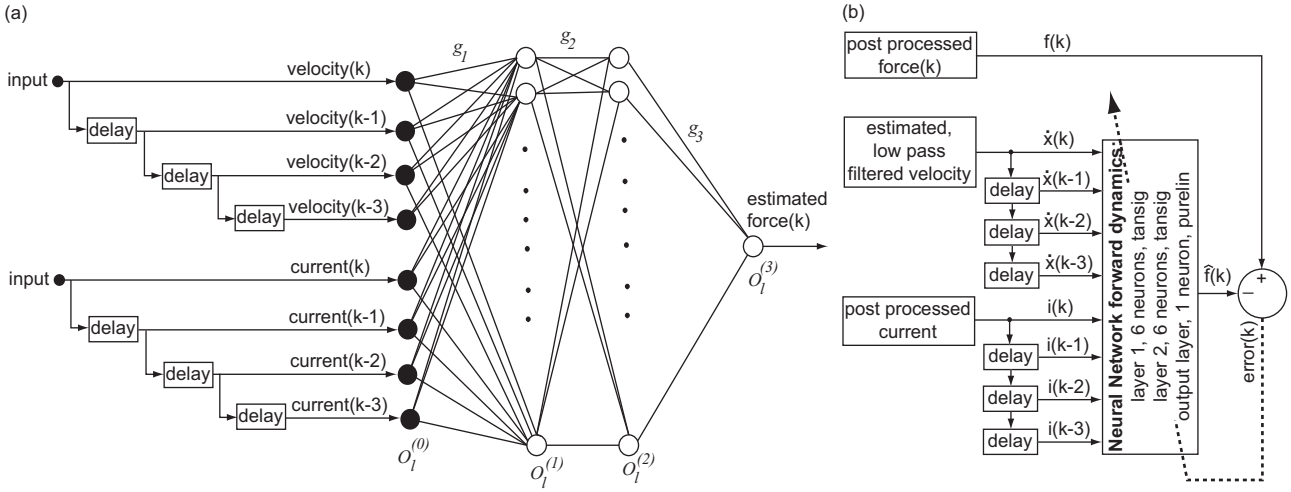

Fig. 6 NN architecture of forward MR damper model and its training

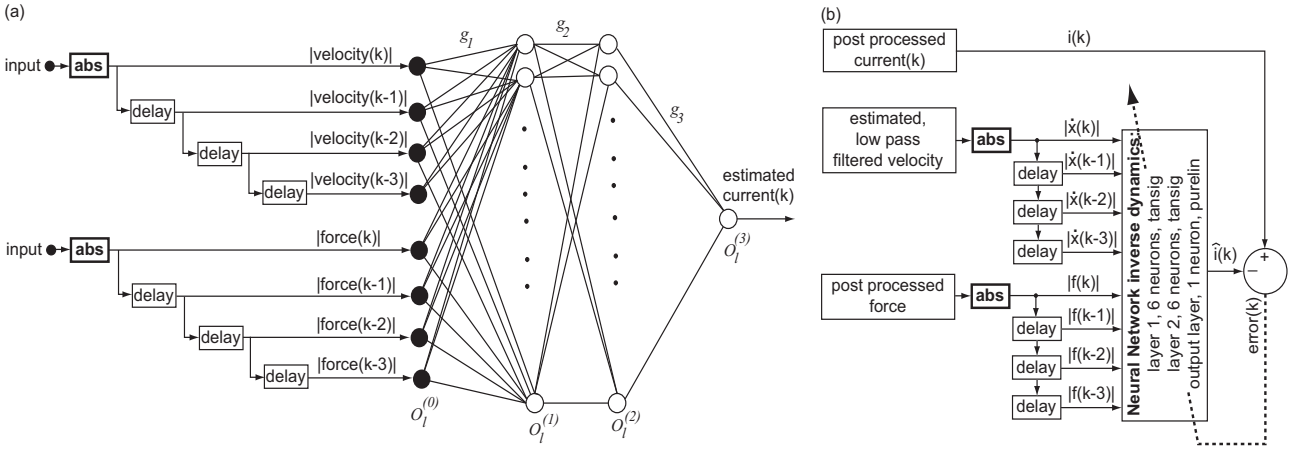

Fig. 7 NN architecture of inverse MR damper model and its training

$$T_l = f(k) \tag{4}$$

where $f(k)$ is the desired force, or in this case the measured force data, at current time state k. The network training was performed using the MATLAB® function *trainlm*. The network has been trained with the input-output data sets obtained from the experiments summarized in Table 1. For training of small-to-medium size networks, the Levenberg-Marquardt algorithm (LM) is fairly efficient. The performance index used for the training of the feed forward neural network is the sum of squares of the difference e_l between the desired target T_l and the actual network output $O_l^{(3)}$

$$V(\mathbf{Z}) = \sum_{l=1}^{I} e_l^2 = \sum_{l=1}^{I} (T_l - O_l^{(3)})^2 \tag{5}$$

where $\mathbf{Z}$ is a vector containing all network weights and bias values to be optimized, while q is the

length of the data set. The LM algorithm updates the parameters based on minimization of the performance index *V*.

3.3 Inverse damper model

Fig. 7 shows the corresponding NN for the inverse damper model with velocity and damper force as input states, and desired damper current as the single output. In order to estimate the MR damper current $\hat{i}(k)$, the NN for the inverse model uses the actual and three previous values of the two input states

$$\hat{i}(k) = NN\begin{bmatrix} |\dot{x}(k)| & |\dot{x}(k-1)| & |\dot{x}(k-2)| & |\dot{x}(k-3)| \\ |f(k)| & |f(k-1)| & |f(k-2)| & |f(k-3)| \end{bmatrix} \tag{6}$$

For the feed forward neural network based inverse dynamics modeling of the MR damper, the network output is $\hat{i}(k) = O_l^{(3)}$ where $\hat{i}(k)$ is the predicted current from the inverse MR model. The target of the inverse neural model

$$T_l = i(k) \tag{7}$$

is the desired damper current $i(k)$, which in this case is the experimentally measured data. The structure of the NN architecture is similar to that of the forward model. However, the output current can only take on positive values, irrespective of the sign of velocity and/or force. Therefore, the NN architecture for the inverse damper model is trained using the absolute values of the two input states. This approach helps to avoid negative spikes in the estimated current when tracking a desired damper force.

4. Model validation

The model validation is carried out for independent and experimentally determined time records. Sections 4.1 and 4.2 consider the NNs of the forward and inverse damper model, respectively, while section 4.3 demonstrates that the presented NNs are able to emulate pure viscous damping.

4.1 Forward model

The forward MR damper model is validated using the validation data sets 1b-19b listed in Table 1. Due to the large amount of validation data, the measured and simulated force displacement trajectories are compared for some selected tests. The selection is made such that the comparison considers all displacement amplitudes, frequencies and damper currents. Figs. 8 and 9 show the result for combinations of constant current values at different displacement amplitudes and driving frequencies. As seen from the figures the NN model is fairly accurate in predicting the forward dynamics of the MR damper. Figs. 10 and 11 show the results for half-sinusoidal current at different amplitudes and frequencies. As can be observed from these figures, the forward MR damper model is able to predict the main characteristics of the MR damper under consideration with fairly good accuracy. The strong current dependent yield force is captured well, the slope of the pre-yield region is estimated very accurately in all cases and the force response due to the

aggregation and radial migration of particles (Boston *et al.* 2010, Weber and Boston 2011a, b), which is visible by the rather slow force increase after the damper rod turns its direction, is also predicted satisfactorily. It is evident that all of the major damper characteristics are predicted significantly better for the half-sinusoidal current in Figs. 10 and 11 than for the constant current case in Figs. 8 and 9. This rather surprisingly fact is related to the transition of the MR damper force from the pre-sliding regime, i.e. pre-yield region, to the sliding regime, i.e. post-yield region, which is more pronounced in the tests made at constant current than at half-sinusoidal current. However, the output of the tangent sigmoid transfer function is almost independent of its input when the MR damper is operated in the post-yield region which corresponds to the almost horizontal part in the force velocity trajectory of MR dampers. Hence, the tangent sigmoid transfer function is not able to precisely capture the fairly slow force increase at constant current due to the aggregation and radial migration of particles which explains the superior model validation results at half-sinusoidal current.

4.2 Inverse model

The inverse MR damper model is also validated using the validation data sets 1b-19b in Table 1. The results for constant current, two different displacement amplitudes and four different displacement frequencies are shown in Figs. 12(a)-(b). The estimated current shows significant local spikes that might arise because the NN architecture has also been trained with half-sinusoidal current data or from the bearing plays of the damper rod joints at zero-crossing of the velocity.

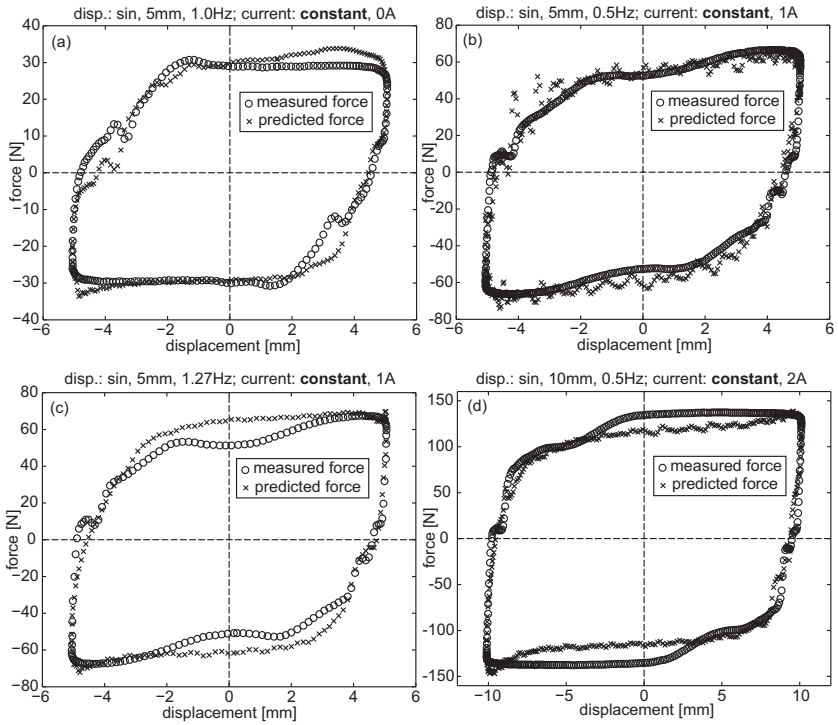

Fig. 8 Validation of forward MR damper model for constant current of 0 A (a), 1 A (b, c) and 2 A (d) and different displacement amplitudes and frequencies

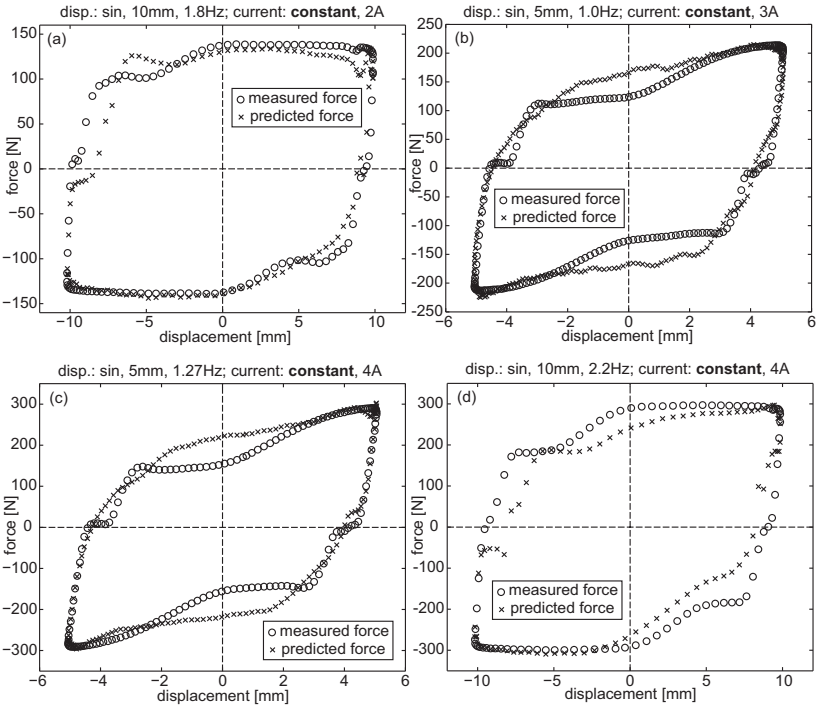

Fig. 9 Validation of forward MR damper model for constant current of 2 A (a), 3 A (b) and 4 A (c, d) and different displacement amplitudes and frequencies

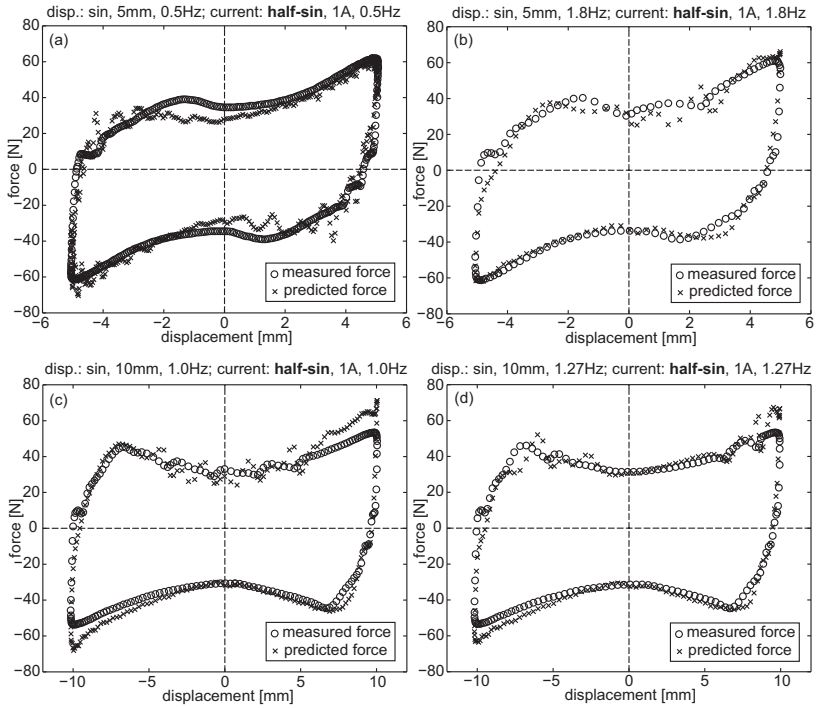

Fig. 10 Validation of forward MR damper model for half-sinusoidal current at 1 A and different displacement amplitudes and frequencies

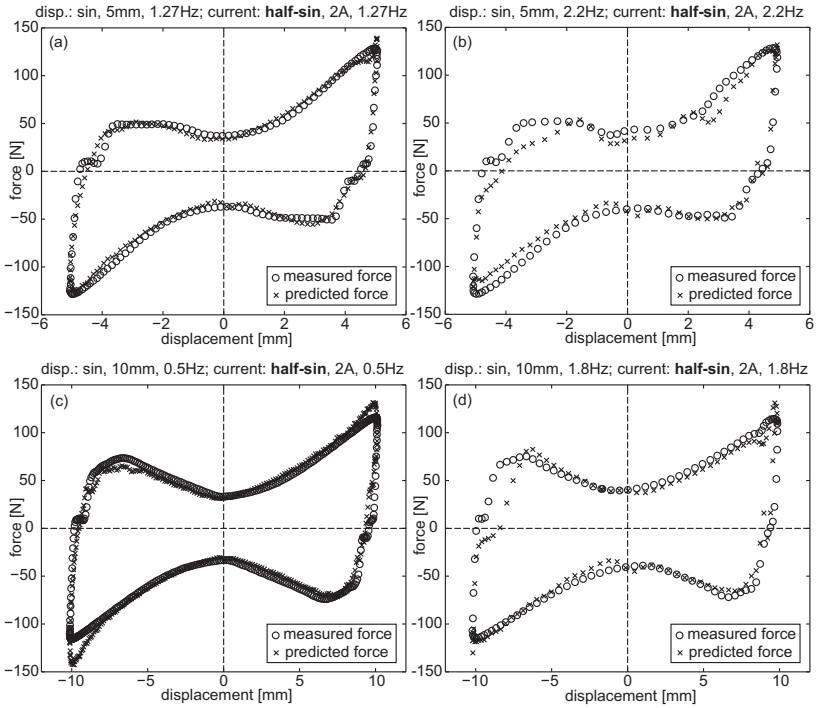

Fig. 11 Validation of forward MR damper model for half-sinusoidal current at 2 A and different displacement amplitudes and frequencies

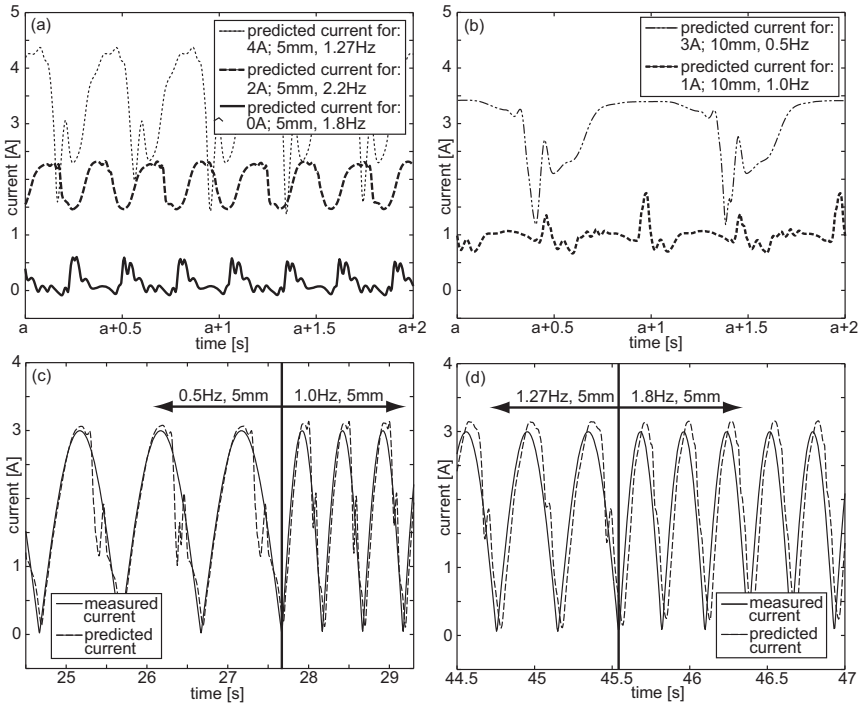

Fig. 12 Validation of inverse MR damper model for constant current (a, b) and half-sinusoidal current at 3 A (c, d)

Although the bearing plays are on the order of 0.02 mm or less, force knocking effects cannot be avoided when the piston of the hydraulic machine turns its direction and thereby the damper force and velocity undergo zero-crossings. This hypothesis is partly verified by the fact that the spikes show the same frequency characteristics as the applied displacement. Similar results have also been reported in Wang and Liao (2005) and Metered *et al.* (2009). This fact might indicate that the NN is fairly sensitive to high frequency signal inputs and has only little low pass behaviour. In contrast to the prediction of constant current, the prediction of the half-sinusoidal current is fairly accurate for different displacement amplitudes, frequencies and current amplitudes as shown in Figs. 12©-(d), 13 and 14. However, also this model validation test shows current spikes and therefore local modelling errors at each half period. Since these spikes occur later than the current maximum, which means after the hydraulic piston has turned its direction, the current spikes cannot result from the force knocking effects at zero velocity crossing, but may instead result from the Stribeck effect, which occurs at the transition between the pre- and post-yield regions and thereby induces a jump in the force. Despite the apparent modelling error due to the spikes of the estimated current, these spikes are rather small compared to e.g. the validation results presented in Wang and Liao (2005). Another reason for the current spikes that occur when the MR damper force gets out of or enters the pre-yield regime might be that the tangent sigmoid transfer function of the hidden layers does not include a hysteresis whereas the measured force velocity trajectory shows a hysteresis due to the pre-yield behaviour. As a result, two different force values exist for the same current and velocity in the measurement data. When training the forward model, the forward model can distinguish between the two different force values because these values can be associated with the different signs in the MR damper displacement since the forward model is not trained with absolute velocity as the inverse model. However, the inverse model is trained with the absolute values of velocity and force. Consequently, the inverse model cannot distinguish between the two different force values in the pre-yield regime – depending if leaving or entering the pre-yield regime – for same velocity and current because the displacement that is derived from velocity does not change its sign. It seems that the inverse model associates the two different force values in the pre-yield regime with two different current values which ends up in the observed current spikes. It is therefore concluded that, although the training of the inverse NN model with absolute values of velocity and force helps to avoid negative current values, shows the drawback that the model cannot distinguish between the different force values in the pre-yield regime. To overcome this drawback could be the adoption of a transfer function with hysteresis in the hidden layers. Last but not least, the current spikes may also be triggered by the fact that the measurement data was split into data sets of 10 steady state cycles that were connected to one training data time history. The 10 steady state cycles were connected at zero crossings of the displacement where the force is not zero. Thus, the force jumps every 10 steady state cycles in the training data and current also shows steps after 50 steady state cycles due to the five tested frequencies, see Fig. 4(b).

4.3 Emulation of viscous damping using validated models

In this section the forward and inverse models are used to demonstrate how accurate pure viscous damping can be emulated by the rotary MR damper of the present study. Fig. 15(a) shows the flow chart of this simulation. The velocity of the MR damper is assumed to be pure sinusoidal. This is a reasonable assumption for damping of lightly damped structures, where the structural response is typically dominated by resonance at the frequency of the critical vibration mode and with a slowly varying amplitude envelope. The desired control force is the product of velocity and

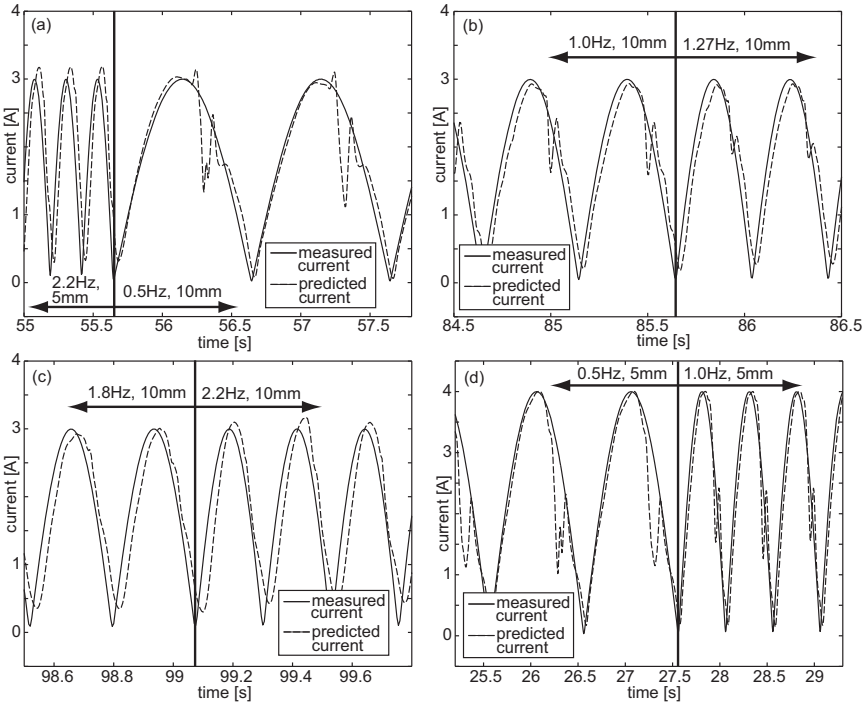

Fig. 13 Validation of inverse MR damper model for half- sinusoidal current at 3 A (a-c) and 4 A (d)

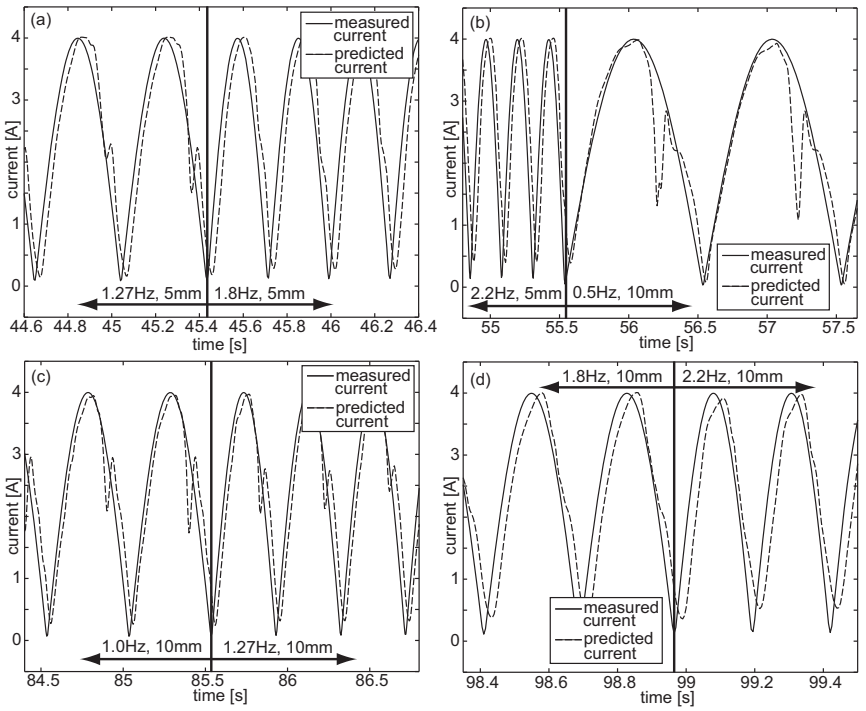

Fig. 14 Validation of inverse MR damper model for half-sinusoidal current at 4 A (a-d)

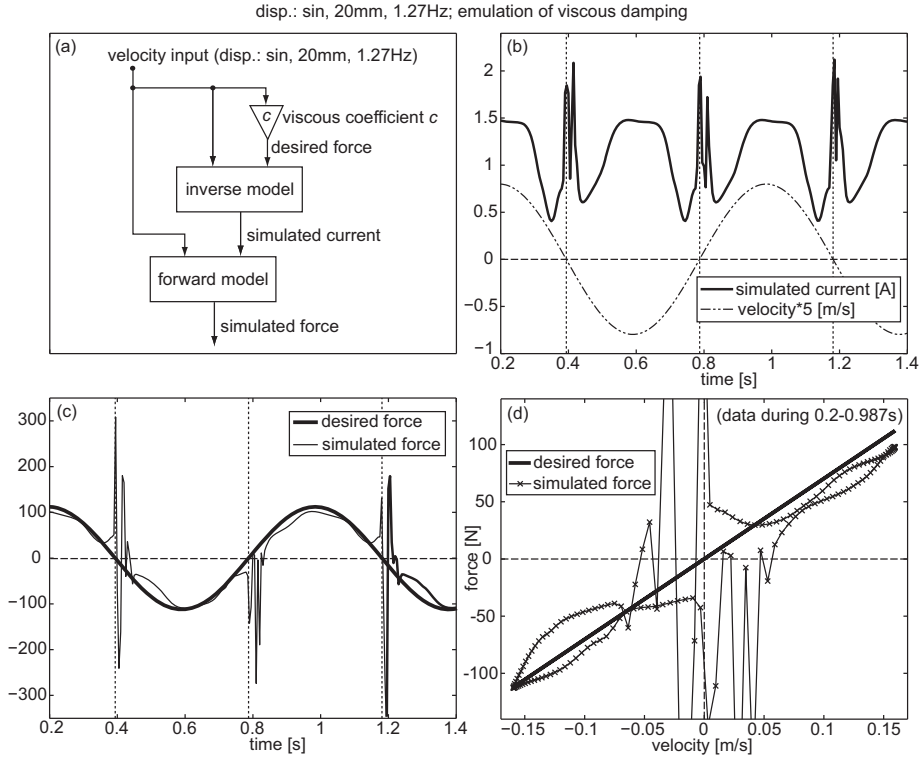

Fig. 15 Simulated emulation of viscous damping: Flow chart (a), simulated MR damper current (b) and simulated MR damper force (c, d)

The viscous coefficient *c*. The damper velocity and the desired control force are used as the input states for the inverse MR damper model, which then estimates the corresponding damper current that is applied to the MR damper in order to generate a pure viscous force. This force is estimated using the forward MR damper model. If the NN for the inverse and the forward MR damper model are sufficiently accurate the simulated damper force should be comparable to the corresponding pure viscous damper force. The simulation results are shown in Figs. 15(b)-(d). The simulated current in Fig. 15(b) exhibits two significant spikes on top of the approximately half-sinusoidal time history. The first spike should not occur because the desired force decreases to zero. Hence, zero current would be the best choice to track the desired viscous force as precise as possible. The second current spike occurs when the MR fluid is operated within the pre-yield region. This spike is therefore needed because the actual MR damper force at 0 A within the pre-yield region is smaller than the desired viscous force that increases rapidly at displacement extremes due to the elliptic force displacement trajectory of viscous damping (Maslanka *et al.* 2007). When the MR fluid is operated in the post-yield region, the current shows approximately a half-sinusoidal behavior because of the pure sinusoidal behavior of the desired force, see Fig. 15(c). The main discrepancies are mainly due to the non-linear relation between yield force and current and the force response, arising because of the inherent migration and aggregation of the particles in the MR fluid (Boston *et al.* 2010, Weber and Boston 2011a, b). Despite the mediocre estimate of the current at zero velocity and the slightly overestimated current during the pre-yield region, the time

history of the damper force in Fig. 15(c) and the force velocity trajectory in Fig. 15(d) demonstrate that pure viscous damping is in fact tracked fairly accurate at velocities larger than 0.05 m/s. The obtained results indicate that the NNs have difficulties to accurately estimating the behavior of the MR damper in the pre-yield region, which produces current spikes and thereby significant force tracking errors at small velocities. However, effective structural damping is mainly governed by the energy dissipation at large velocities, why these low-velocity current spikes are only of minor importance for most practical applications.

5. Conclusions

This paper describes the feed forward back propagation neural network based modeling of the forward and the inverse behavior of a rotary MR damper using experimentally measured data for both training and validation. The measured data has been low pass filtered in order to remove high frequency signal parts that might have significant influence on the performance of the NN. The measured data comprising two displacement amplitudes, five frequencies and both constant and half-sinusoidal current has been combined to get a single sequential time history and afterwards down-sampled from 1000 Hz to 200 Hz to optimize the training of the NN architecture. An optimization procedure has been presented to identify the NN architecture that minimizes the error of the forward model. For training the procedure has been tested with combinations of measured displacement, velocity, acceleration and damper current as input states. Furthermore, the number of previous values of the input states and the number of hidden layers and neurons have been altered to obtain the best numerical fit. To limit the computational time of this numerical optimization, the transfer functions for the hidden and output layers were fixed to the tangent sigmoid function and the linear function, respectively. The present procedure demonstrates that the modeling error is not decreased significantly:

- if displacement and acceleration are taken as inputs in addition to velocity, and
- if substantially more than three past values of the inputs are taken into account, and
- if substantially more than two hidden layers of more than six neurons are considered.

The same NN architecture has also been used to model the inverse MR damper behavior. In this case the damper current is the output, while the absolute values of damper force and velocity are used as input states. The introduction of the absolute values as the input to the NN minimizes the possibility of negative spikes in the estimated damper current when e.g. tracking a desired viscous force.

The trained forward and inverse MR damper models have been validated with measurement data that is independent of the training data at different displacement amplitudes and frequencies. The validation data comprises test records at two displacement amplitudes, five frequencies and both constant and half-sinusoidal damper current signals. The validation shows that the forward model is able to predict the MR damper force with high accuracy. Especially the force response due to the migration and aggregation of the MR fluid particles is captured well, and the slope of the force displacement trajectory in the pre-yield region is predicted accurately. The validation of the inverse MR damper model shows two particular characteristics. When the measurement data has been obtained from constant current, the predicted current records contain significant spikes with the same frequency as the damper displacement. This might therefore result from force knocking effects at displacement extremes due to the inherent bearing plays between the damper rod and the hydraulic machine, which are of the order of 0.02 mm. For these tests, only the mean

value of the predicted current is accurate. In contrast, the prediction based on the half-sinusoidal current turns out to give more accurate results for all amplitudes and frequencies used in the tests. Nevertheless, also this validation shows current spikes which do not occur at the time of displacement extremes, but later. This indicates that these spikes are forced by the Stribeck effect, which occurs between the pre- and post-yield regions.

The validated forward and inverse MR damper models are finally used to simulate the emulation of viscous damping. The simulation shows that the inverse model overestimates the current in the vicinity of zero velocity, i.e. in the pre-yield region, while the output current is quite accurate within the post-yield region. As a result, the force tracking error is fairly large at small damper velocities, but considerably smaller at velocities where the MR damper is not operated in the pre-yield region.

This investigation shows that the NN technique can be used to model the inverse MR damper behavior and thereby effectively solve the force tracking task with sufficiently small force tracking error.

Acknowledgements

The work is supported via the research grant *Damping of Flexible Structures by Smart Control of Semi Active Devices* by the Danish Council of Research and Innovation. The authors also gratefully acknowledge the use of the testing facilities as well as the technical assistance of Empa, Swiss Federal Laboratories for Materials Science and Technology, Dübendorf, Switzerland, and the technical support of the industrial partner Maurer Söhne GmbH & Co. KG, Munich, Germany.

References

Aguirre, N., Ikhouane, F., Rodellar, J., Wagg, D.J. and Neild, S.A. (2010), "Viscous and Dahl model for MR dampers characterization: A Real time hybrid test (RTHT) validation", *Proceedings of the 14th European Conference on Earthquake Engineering*, August - September, Ohrid, Republic of Macedonia.

Boston, C., Weber, F. and Guzzella, L. (2010), "Modeling of a disk-type magnetorheological damper", *Smart Mater. Struct.*, **19**(4), 045005.

Chang, C. and Roschke, P. (1998), "Neural network modeling of a magnetorheological damper", *Journal of Intelligent Material Systems and Structures*, **9**(9), 755-764.

Chang, C. and Zhou, L. (2002), "Neural network emulation of inverse dynamics for a magnetorheological damper", *Journal of Structural Engineering*, **128**(2), 231-239.

Christenson, R.E., Spencer, Jr. B.F. and Johnson, E.A. (2006), "Experimental verification of smart cable damping", *Journal of Engineering Mechanics*, **132**(3), 268-278.

Dominguez, A., Sedaghati, R. and Stiharu, I. (2004), "Modelling the hysteresis phenomenon of magnetorheological dampers", *Smart Mater. Struct.*, **13**(6), 1351-1361.

Dominguez, A., Sedaghati, R. and Stiharu, I. (2006), "A new dynamic hysteresis model for magnetorheological dampers", *Smart Mater. Struct.*, **15**(5), 1179-1189.

Ikhouane, F. and Dyke, S. (2007), "Modeling and identification of a shear mode magnetorheological damper", *Smart Mater. Struct.*, **16**(3), 605-616.

Jiménez, R. and Alvarez-Icaza, L. (2005), "LuGre friction model for a magnetorheological damper", *Journal of Structural Control and Health Monitoring*, **12**(1), 91-116.

Lee, H., Jung, H., Cho, S. and Lee, I. (2008), "An experimental study of semiactive modal neuro-control scheme using MR damper for building structure", *Journal of Intelligent material Systems and Structures*,

19(9), 1005-1015.
Li, H., Liu, M., Li, J., Guan, X. and Ou, J. (2007), "Vibration control of stay cables of the Shandong Binzhou yellow river highway bridge using magnetorheological fluid dampers", *Journal of Bridge Engineering*, **12**(4), 401-409.
Maslanka, M., Sapinski, B. and Snamina, J. (2007), "Experimental study of vibration control of a cable with an attached MR damper", *Journal of Theoretical and Applied Mechanics*, **45**(4), 893-917.
Metered, H., Bonello, P. and Oyadiji, S.O. (2009), "The experimental identification of magnetorheological dampers and evaluation of their controllers", *Journal of Mechanical Systems and Signal Processing*, **24**(4), 976-994.
Neelakantan, V.A. and Washington, G.N. (2008), "Vibration control of structural systems using MR dampers and a 'modified' sliding mode control technique", *Journal of Intelligent Material Systems and Structures*, **19**(2), 211-224.
Sahin, I., Engin, T. and Cesmeci, S. (2010), "Comparison of some existing parametric models for magnetorheological fluid dampers", *Smart Mater. Struct.*, **19**(3), 035012.
Shulman, Z.P., Korobko, E.V., Levin, M.L. *et al*. (2006), "Energy dissipation in electrorheological damping devices", *Journal of Intelligent Material Systems and Structures*, **17**(4), 315-320.
Sims, N.D., Holmes, N.J. and Stanway, R. (2004), "A unified modelling and model updating procedure for electrorheological and magnetorheological vibration dampers", *Smart Mater. Struct.*, **13**(1), 100-121.
Soeiro, F.J., Stutz, L.T., Tenenbaum, R.A. and Neto, A.J. (2008), "Stochastic and hybrid methods for the identification in the Bouc-Wen model for magneto-rheological dampers", *Journal of Physics: conference series*, **135**, 012093.
Spencer, Jr. B.F. and Nagarajaiah, S. (2003), "State of the art of structural control", *Journal of Structural Engineering*, **129**(8), 845-856.
Tse, T. and Chang, C. (2004), "Shear-mode rotary magnetorheological damper for small-scale structural control experiments", *Journal of Structural Engineering*, **130**(6), 904-910.
Tsoukalas, L. and Uhrig, R. (1997), *Fuzzy and Neural Approaches in Engineering*, John Wiley & Sons Inc.
Wang, D.H. and Liao, W.H. (2005), "Modeling and control of magnetorheological fluid dampers using neural networks", *Smart Mater. Struct.*, **14**(1), 111-126.
Weber, F., Feltrin, G. and Motavalli, M. (2005), "Passive damping of cables with MR dampers", *Journal of Materials and Structures*, **38**(279), 568-577.
Weber, F., Feltrin, F. and Distl, H. (2008), "Detailed analysis and modeling of MR dampers at zero current", *Structural Engineering Mechanics*, **30**(6), 787-790.
Weber, F., Distl, H., Feltrin, G. and Motavalli, M. (2009), "Cycle energy control of MR dampers on cables", *Smart Mater. Struct.*, **18**(1), 015005.
Weber, F. and Boston, C. (2011a), "Measured tracking of negative stiffness with MR damper", *Proceedings of the 5th ECCOMAS Thematic Conference on Smart Structures and Materials*, July, Saarbrücken, Germany.
Weber, F. and Boston, C. (2011b), "Clipped viscous damping with negative stiffness for semi-active cable damping", *Smart Mater. Struct.*, **20**(4), 045007.
Weber, F., Boston, C. and Maslanka, M. (2011c), "An adaptive tuned mass damper based on the emulation of positive and negative stiffness with an MR damper", *Smart Mater. Struct.*, **20**(1), 015012.
Weber, F. and Maslanka, M. (2012), "Frequency and damping adaptation of a TMD with controlled MR damper", *Smart Mater. Struct.*, **21**(5), 055011.
Weber, F. (2013a), "Bouc-Wen model-based real-time force tracking scheme for MR dampers", *Smart Mater. Struct.*, **22**(4), 045012.
Weber, F., Bhowmik, S. and Høgsberg, J. (2013b), "Extended Neural Network Based Scheme for Real-Time Force Tracking with MR Dampers", *Structural Control and Health Monitoring*, doi: 10.1002/stc.1569.
Won, J.-S. and Sunwoo, M. (2009), "Fuzzy modelling approach to magnetorheological dampers: forward and inverse model", *Proc. of the Inst. of Mech. Eng. Part I – Journal of Systems and Control Engineering*, **223**(I8) 1055-1066.
Wu, W.J. and Cai, C.S. (2010), "Cable vibration control with a semiactive MR damper - numerical

simulation and experimental verification", *Structural Engineering and Mechanics*, **34**(5), 611-623.
Xia, P. (2003), "An inverse model of MR damper using optimal neural network and system identification", *Journal of Sound and Vibration*, **266**(5), 1009-1023.
Xiaomin, X., Qing, S., Ling, Z. and Bin, Z. (2009), "Parameter estimation and its sensitivity analysis of the MR damper hysteresis model using a modified genetic algorithm", *Journal of Intelligent Material Systems and Structures*, **20**(17), 2089-2100.
Yang, G., Spencer, Jr. B.F., Jung, H.J. and Carlson, J.D. (2004), "Dynamic modeling of large-scale magneto-rheological damper systems for civil engineering applications", *Journal of Engineering Mechanics*, **130**(9), 1107-1114.
Yang, F., Sedaghati, R. and Esmailzadeh, E. (2009), "Development of LuGre friction model for large-scale magneto-rheological fluid damper", *Journal of Intelligent Material Systems and Structures*, **20**(8) 923-937.
Ye, M. and Wang, X. (2007), "Parameter estimation of the Bouc-Wen hysteresis model using particle swarm optimization", *Smart Mater. Struct.*, **16**(6), 2341-2349.